36E.0 IN-SITU CHARACTERIZATION OF MICROSTRUCTURAL EVOLUTION DURING SIMULATED ADDITIVE MANUFACTURING IN MODEL ALLOYS

Brian Rodgers (Mines)
Faculty: Amy Clarke (Mines)
Industrial Mentor: TBD

This project initiated in Fall 2019 and is supported by a Multidisciplinary University Research Initiative (MURI) project funded by the Office of Naval Research (ONR). The research performed during this project will serve as the basis for a Ph.D. thesis program for Brian Rodgers.

36E.1 Project Overview and Industrial Relevance

Laser Powder Bed Fusion (L-PBF) Additive Manufacturing (AM) is an attractive technology for the manufacture of turbine and aerospace components. However, the processing effects of L-PBF on microstructural evolution are not well understood. This project will develop fundamental understanding of solidification phenomena under AM conditions in model alloys. Emphasis is placed on in-situ experimentation at the Advanced Photon Source (APS) at Argonne National Laboratory (ANL) and Dynamic Transmission Electron Microscopy (DTEM) at Lawrence Livermore National Laboratory (LLNL) with model alloys to understand the role of rapid solidification and processing history on microstructural development. If the solidification behavior during L-PBF is sufficiently understood, it may be possible to manufacture highly oriented, “single crystal” turbine components by AM, for example.

The alloy systems chosen are two model ternary Ni-base superalloys with different Mo and Al contents, but identical equilibrium γ’ volume fractions, and the Al-Ag system. The nickel alloys are referred to as R2 and R4 and are single crystals of known orientation. R2 and R4 were chosen for their closer resemblance to industrially-relevant nickel-based alloys, and the Al-Ag system was chosen because it demonstrates strong chemical segregation behavior, since the solidus and liquidus have shallows slopes in this system.

36E.2 Previous Work – Sample Preparation and Project Onboarding

In-situ experimentation at the APS has been performed, and highly specific sample preparation was completed prior to these experiments. Training has also been completed to perform *ex-situ* characterization of the APS samples.

36E.3 Recent Progress

36E.3.1 APS *In-Situ* Experiments

Samples of the R2, R4, Al-10%Ag, and Al-18%Ag alloys were taken to the APS for *in-situ* experimentation. Compositions are shown in **Table 36E.1**. The experiments consisted of impinging the top side of a thin sample with a laser to create a molten pool while simultaneously providing a flux of high energy X-rays that transverse though the flat side of the sample to allow for *in-situ* imaging of the molten pool and subsequent solidification. The laser parameters used are similar to that of the L-PBF process, which is the process simulated with the APS AM simulator.

Two types of experiments were performed for the Ni-base alloys; one with overlapping spots and the other with individual rasters of identical heat input. These experiments were strategically designed to complent earlier work. Crystal orientation was chosen such that the ⟨100⟩, ⟨110⟩, or ⟨111⟩ directions were parallel to the laser beam for all of the trials. The first spot in all of the overlapping spot trials was done at a lower power, which previous experiments on these alloys have shown to create newly nucleated equiaxed grains at the top of the melt pool after solidification. With equiaxed grains created at the top of the spot melt after solidification, the edge of the second spot melts and then intersects the middle of the first spot melt to see if the grains will epitaxially grow into the second spot melt during solidification. Secondary spot melts were performed with either identical power to the first spot melts, or at an increased power which previous experiments have shown to not nucleate new equiaxed grains. Parameters for the raster experiments had to be adjusted because the highest power and higher raster speed

experiment caused keyholing, which leads to a different heat input due to the increased coupling efficiency. Experimental Parameters are summarized in **Table 36E.2**.

The Al-Ag system experiments consisted of spot melts at varying powers, rasters, and re-rasters. Re-rasters involved rastering the beam over a region and then rastering the beam over the same region again with identical parameters to re-melt the previous raster. This was done to emulate previous experiments with DTEM of this alloy. In the DTEM experiments, unique microstructures were seen when the same region was re-melted and solidified. These microstructures were different than the microstructure created from the first solidification event. It is believed that the minimal convective fluid flow in the DTEM experiments changes the local chemical segregation resulting in interesting microstructural development that is still being explored. Re-rastering allows for similar solidification velocities, but in a three-dimensional sample which should have increased convective fluid flow. The comparison of DTEM to APS experiments varying convective mass flow will help to prove or disprove that a lack of liquid state mixing is the cause of the unique microstructures seen in the DTEM re-melts.

36E.3.2 Simulation of APS Parameters

The experimental parameters for rasters used at the APS were simulated using a Rosenthal-type approach in MATLAB with formulae found in the literature [36E.1]. The formulae used are **Equations 36E.1-5**.

$$T = T_o + \frac{\lambda P}{2\pi k r}\exp\left(-\frac{v(r+x)}{2\alpha}\right) \tag{36E.1}$$

$$\frac{\partial T}{\partial x} = -\frac{\lambda P v}{4\pi k \alpha r}\left[1 + \frac{x}{r} + \frac{2\alpha x}{v r^2}\right]\exp\left(-\frac{v}{2\alpha}(x+r)\right) \tag{36E.2}$$

$$\frac{\partial T}{\partial y} = -\frac{\lambda P v y}{4\pi k \alpha r^2}\left[1 + \frac{2\alpha}{v r}\right]\exp\left(-\frac{v}{2\alpha}(x+r)\right) \tag{36E.3}$$

$$\frac{\partial T}{\partial t} = \frac{\lambda P v^2}{4\pi k \alpha r}\left[1 + \frac{x}{r} + \frac{2\alpha x}{v r^2}\right]\exp\left(-\frac{v}{2\alpha}(x+r)\right) \tag{36E.4}$$

$$R_\theta = \frac{{}^{\partial T}/_{\partial t}}{\sqrt{\left({}^{\partial T}/_{\partial x}\cos(\theta)\right)^2 + \left({}^{\partial T}/_{\partial y}\sin(\theta)\right)^2}} \tag{36E.5}$$

Where T is temperature in absolute units, T_o is the preheat temperature, λ is coupling efficiency, P is power, v is raster speed, k is thermal conductivity, r is radial distance from the point source, α is thermal diffusivity, x is position along the travel direction from the point source, y is the depth away from the point source, and R_θ is the solidification velocity at an angle from the travel direction. Rosenthal-type solutions assume a semi-infinite geometry, point heat source, no convection, no latent heat of fusion, and identical thermophysical properties in the solid and liquid. Out of these assumptions, the semi-infinite geometry and lack of convection are the most problematic; the difference in properties between solid and liquid are not that great, and a laser is as close to a point heat source as is reasonably achievable. Automatic filtering logic was added to the code to saturate any temperature values greater than twice the absolute melting temperature because the equations used have a singularity at the point heat source.

Values for thermophysical parameters in alloys similar enough to the alloys used are readily available in databases such as matweb, but values for laser absorptivity are not. Instead, absorptivity is treated as a calibratable parameter and is adjusted in the simulation of each melt pool, so that the depth of the molten pool matches the depth of melt pool seen in the APS experiments. This analysis does not capture the effects of keyholing. However, keyholing primarily occurred in the spot melts. Parameters were chosen to avoid keyholing for the Ni-base alloys, and the Al-Ag alloys which experienced keyholing had a conduction mode region before the keyhole initiated. The shape of the simulated and actual pool still does not match perfectly, which is likely caused by the lack of accounting for convection. Simulated pools are sometimes longer than their real-world counterparts because convection increases the rate of heat transfer so the volume of material that is above the melting point shrinks, leading to a smaller molten pool. Some simulated pools are shorter than real-world because the semi-infinite assumption is not true for these

samples, so there was less heat extraction than simulated. Real melt pools in nickel are on average shorter while melt pools in aluminum tend to be longer than the simulated melt pools as a result. A comparison of simulated and measured pool shapes is provided in **Figure 36E.1**.

36E.4 Plans for Next Reporting Period

Ex-situ analysis of the APS samples will be conducted. Analyses will include:

- Top-down imaging of the as-solidified melts;
- More sophisticated simulation using FLOW-3D to capture keyholing and convection;
- Transverse and longitudinal imaging and EBSD of the rasters;
- Imaging and EBSD of the center of spots melts with 'longitudinal' sections for overlapping spots.

36E.5 References

[36E.1] P. Promoppatum, S.-C. Yao, P.C. Pistorius, A.D. Rollett, A Comprehensive Comparison of the Analytical and Numerical Prediction of the Thermal History and Solidification Microstructure of Inconel 718 Products Made by Laser Powder-Bed Fusion, Engineering. 3 (2017) 685–694. doi:10.1016/j.eng.2017.05.023.

36E.6 Figures and Tables

Table 36E.1: Compositions of alloys chosen.

	Ni	Al	Mo	Ag
R2	balance	6.6	1.9	N/A
R4	balance	2.8	22.2	N/A
Al-10Ag	N/A	balance	N/A	10
Al-18Ag	N/A	balance	N/A	18

Table 36E.2: Summary of laser parameters used in experiments at APS. Pulse duration was one ms for all spot melts. Parameters for overlapping melts are shown with a forward dash between the parameters for each.

Alloy	Beam power [W]	Raster speed [m/s]	Notes
R2 [110], R2 [111], R4[100], R4 [110]	253.9	1.6	
	139.4	0.5	
	47.8	0.1	
	82.1/82.1	Spot melt	Edge of second pool intersects middle of first
	82.1/253.9	Spot melt	
R2 [110]	517.1	1.6	
	253.9	1	
R4 [100]	517.1	1.6	
	368.3	1.6	
	253.9	Spot melt	
Al-10Ag & Al-18Ag	282.5/282.5	0.1/0.1	Re-rasters with 100% overlap
	368.3/368.3	2/2	
	282.5	0.1	
	368.3	2	

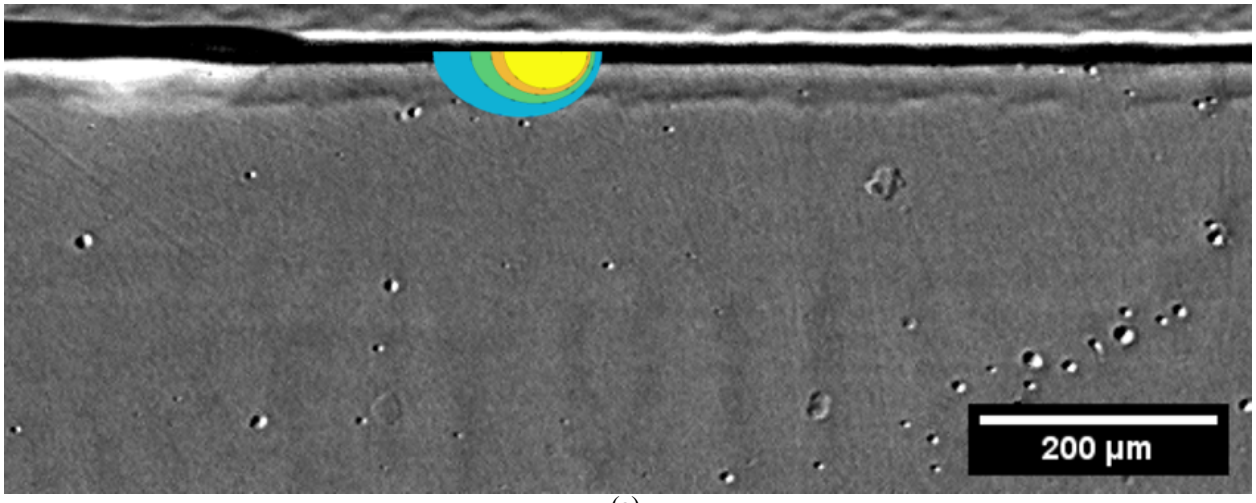

(a)

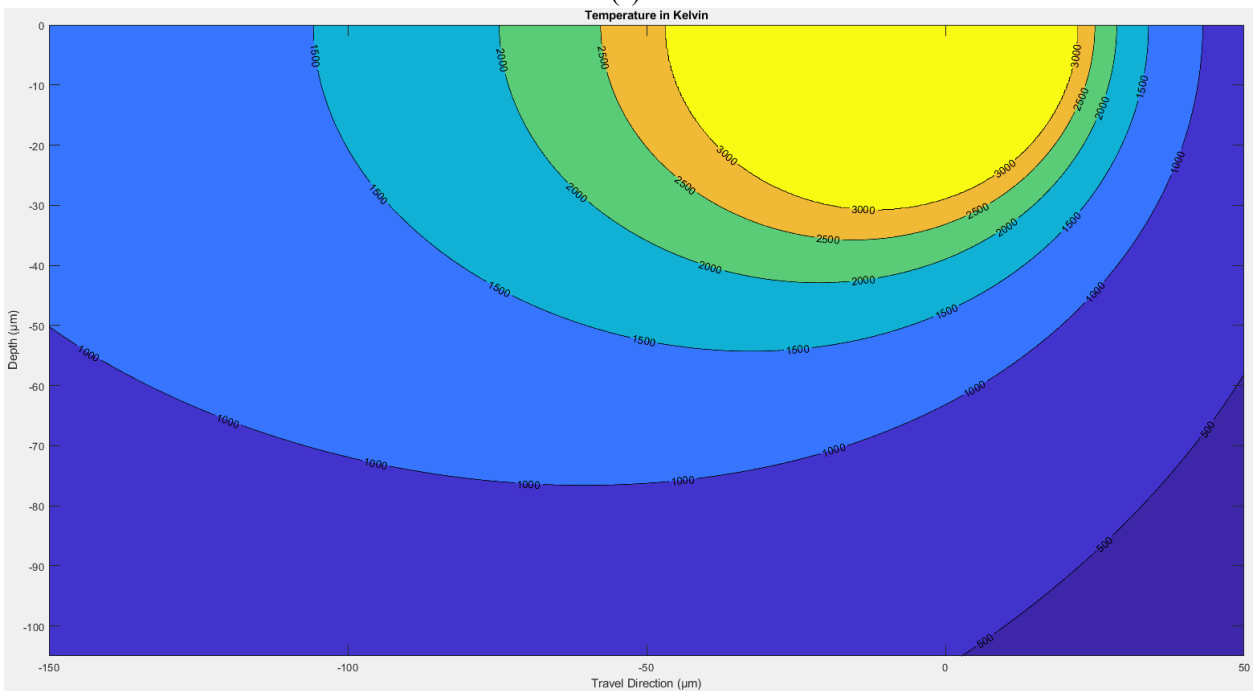

(b)

Figure 36E.1: Comparison of melt pool size and geometry between real with overlaid simulated melt pool (a) and simulated (b) data for Ni-base single crystal samples with ⟨100⟩ directions oriented parallel to the laser direction. The 1500 Kelvin isotherm corresponds to the location of the liquidus